Recent results from the PAMELA experiment

S. B. Ricciarini* on behalf of the PAMELA collaboration

INFN, Structure of Florence,
via G. Sansone 1, Sesto Fiorentino, 50019, Italy
**E-mail: ricciarini@fi.infn.it*

Since July 2006 the PAMELA experiment on satellite is continuously collecting data on several cosmic ray species, in the energy range from tens of MeV to hundreds of GeV. Here results will be presented of the most recent and refined data analyses, in particular those involving observations of interest for indirect dark-matter searches, and with a specific aim at illustrating how the various sources of systematic errors have been taken into account in the measurements.

Keywords: PAMELA; Space Experiment; Cosmic Rays; Antiparticles.

1. Introduction

PAMELA[1] is a satellite-borne experiment designed to study charged particles in the cosmic rays, specifically aimed at identifying the antiparticle component. It has been designed to obtain an unprecedented precision in the measurement of the energy spectra of antiprotons between 80 MeV and 180 GeV, positrons in the range 50 MeV – 270 GeV, and additionally to obtain high-precision spectra of protons, light nuclei ($Z < 8$) and electrons. The main purposes of these measurements are to test cosmic-ray propagation models and to search for evidence of dark-matter particles annihilations or other unknown primary sources.

PAMELA is also able to search for direct evidence of anti-nuclei, with a design sensitivity in the $\overline{\mathrm{He}}/\mathrm{He}$ ratio better than $\sim 10^{-7}$. Moreover, the quasi-polar orbit and low geomagnetic cut-off experienced by the PAMELA apparatus, combined with its intrinsic ability to measure low momenta, allows phenomena connected with Sun activity and Earth magnetosphere to be investigated.

This paper constitutes a review of the recently obtained results, published or near to publication. Only a short summary of the various items involved can be given here; for further details, the reader is referred to

the papers cited in the bibliography and to future publications. Sec. 2 describes the main characteristics of the PAMELA apparatus and of the data analysis criteria employed. The recently published results on positrons and antiprotons are presented and discussed in Sec. 3 and Sec. 4, respectively. A general discussion of the analysis methods developed for the measurement of the absolute fluxes of H and He is given in Sec. 5. Finally, the last section contains some concluding remarks and a general outlook on the items currently under analysis, which will form the argument of future publications by the PAMELA collaboration.

2. PAMELA apparatus and performances

PAMELA (see Fig. 1) is housed inside a pressurized Al vessel filled with N_2 at 1 atm, with thickness of 2 mm in correspondence of the PAMELA acceptance window, and installed on-board of the Resurs-DK1 satellite, which follows an orbit with altitude varying between 350 and 600 km and inclination of 70°. PAMELA is in continuous data acquisition mode since July 2006; the mission is foreseen to last until the end of 2011.

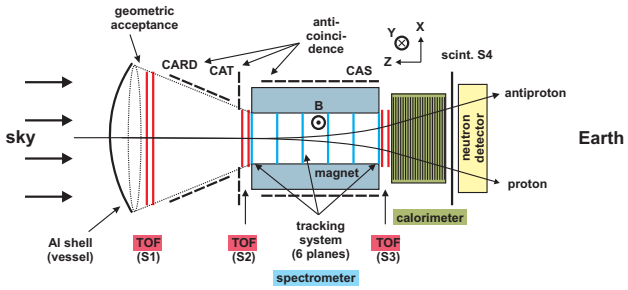

Fig. 1. Schematic view of the PAMELA apparatus, with the indication of the main direction of the magnetic field inside the spectrometer cavity. PAMELA is 1.3 m long and less than 1 m wide.

The core of the PAMELA apparatus is formed by a high-precision magnetic spectrometer: a 140 kg permanent magnet produces an approximately uniform and dipolar magnetic field of ≈ 0.4 T in a $16 \times 13 \times 44$ cm^3 rectangular cavity, equipped with a tracking system composed of six equidistant planes of double-sided microstrip Si detectors. Each Si sensor is 300 μm thick, 5.3×7.0 cm^2 wide, with a read-out pitch of 51.0 and 66.5 μm on the junction and ohmic side, respectively, thus providing two independent

impact coordinates. The cavity dimensions and magnetic field define a geometrical factor of 21.6 cm^2 sr.

The magnetic spectrometer determines the sign of the electric charge Ze of the incident particle and its magnetic deflection $\eta = Ze/Pc$ (where Pc is the particle momentum in GeV) and rigidity $R = 1/|\eta|$. The deflection resolution depends on the spatial resolution of the Si detectors and on the precision in the knowledge of the relative positions of the Si sensors. The former has been directly measured at beam tests and amounts to 3 (12) μm for the junction (ohmic) side, for normally incident trajectories; the Si sensor positions after launch have been determined with an *in-flight* alignment procedure using the collected relativistic p, e^- and e^+, validated at beam tests and characterized by a precision better than 1 μm.

For relativistic particles, the average deflection uncertainty $\delta\eta$ is constant with particle energy (corresponding to a $\delta R/R \propto R$) and it is usually expressed in terms of the maximum detectable rigidity MDR, defined as the rigidity for which the relative uncertainty is 100% ($MDR = 1/\delta\eta$). The MDR is evaluated through the track fitting algorithm and varies on an event basis: it depends on the number and distribution of fitted points and on the magnetic field intensity along the trajectory; it also varies with the track inclination in the Si sensors and the noise of the hit microstrips, both affecting the spatial resolution of the single position measurements. From measurements at beam tests, the MDR distribution exceeds 1 TV.

The time-of-flight (ToF) system comprises six layers of fast plastic scintillators, segmented into paddles with independent PMT read-out, and arranged in three double planes (S1, S2 and S3). Coincidental energy deposits in combinations of layers provide the main trigger for the experiment. Time-of-flight information is combined with spectrometer track-length information to determine particle velocities. The measured time-of-flight resolution, better than 300 ps, allows e^-/e^+ to be separated from $p/\overline{p}$ up to an energy of $\sim$ 1 GeV. Upward-going (i.e. *albedo*) particles are rejected with a significance of 60 standard deviations.

Ionization measurements in the scintillator layers and Si sensors allow the absolute value of particle charge to be determined at least up to Z = 7 and 5, respectively.

The sampling electromagnetic calorimeter is composed of 22 modules, each one formed by a central plate of W absorber surrounded by 2 single-sided Si strip planes, for a total depth of 16.3 radiation lengths and 0.6 nuclear interaction lengths. Each Si plane is composed of nine 380 μm thick, 8×8 cm^2 wide sensors with 2.4 mm strip read-out pitch. The main

task of the calorimeter is to discriminate e^+ (e^-) from p ($\overline{p}$); the longitudinal and transverse segmentation of the calorimeter, combined with the measurement of the energy deposited on each Si strip, allows a high identification (or rejection) power for electromagnetic showers against interacting and non-interacting hadrons (see also Sec. 3).

The anti-coincidence (AC) system consists of four plastic scintillators (CAS) surrounding the sides of the magnet, one (CAT) covering the top and four (CARD) delimiting the volume between the first two ToF planes. The main purpose of the AC system is to identify events characterized by secondary particles produced in the apparatus.

The following list summarizes the "basic" event selection criteria which have been generally applied to identify clean events with primary particle of galactic origin:

- single reconstructed trajectory in the spectrometer, entirely contained in a chosen fiducial acceptance, with good quality (number of hits, track fit χ^2) for a proper rigidity measurement;
- cut on the event MDR, depending on the particle rigidity R, R<MDR/n (or equivalently $\delta\eta < |\eta|/\mathrm{n}$), to select events with enough precisely measured deflection;
- no spurious signals from multi-particle events in the ToF and AC scintillators above the tracking system;
- ionization releases consistent with particle energy, for the selected Z;
- down-going particle, with rigidity exceeding the vertical Stoermer geomagnetic cut-off (estimated on the basis of the satellite position) by a safety factor (1.3), thus taking into account the uncertainties associated to the model of the Earth magnetosphere.

Additional cuts are required for rare particles, as discussed in Sec. 3 and 4. All the employed analysis techniques have been validated through extended cross-checks between *in-flight* measurements and custom Monte Carlo simulations, based on GEANT3[2] code (and also FLUKA[3] for what concerns hadronic interactions) and tuned by means of data from several beam tests.

3. Positron fraction

The most important aspect to be considered for the measurement of the positron fraction (i.e. the e^+ flux divided by the sum of e^+ and e^- fluxes) is to keep under control the proton contamination in the positron sample; this contamination is related to $\pi_0 \rightarrow \gamma\gamma$ decays in hadronic showers, which can

mimic electromagnetic showers; moreover, the p/e^+ ratio increases with the particle rigidity, being $\sim 10^3$ at 1 GV and $\sim 10^4$ at 100 GV.

In our conservative approach, the residual proton contamination is quantified by using only *in-flight* data, without any dependence on simulations or beam-test data. Precisely, a nearly pure proton sample is obtained by requiring non-interacting particles in the upper 2 (out of 22) calorimeter modules; the selection cuts for e^+ are then applied to calorimeter variables evaluated in the "restricted" calorimeter formed by the lower 20 modules. On the other side, e^+ (with residual p contamination) and e^- samples, with charge sign given by the spectrometer, are selected by using the same calorimeter variables and selection cuts, applied to the completely equivalent "restricted" calorimeter formed by the upper 20 modules.

For what concerns the chosen selection criteria, studies with particle beams and simulations showed[4] that PAMELA achieves a proton rejection power better than 10^5 up to an energy of $\sim$ 200 GeV, with a positron selection efficiency of 80%, when employing suitably strong cuts, based on the topology of the shower inside the calorimeter, and when requiring the match between the total energy release detected in the calorimeter and the momentum given by the spectrometer.

A parametric bootstrap analysis with maximum likelihood fitting is performed on the three distributions obtained with the previously outlined method (see Fig. 2), for a number of rigidity intervals, and the amounts of detected electrons, positrons and contaminating protons are thus determined. As a cross-check, a non-parametric statistical analysis gives consistent results, well within one standard deviation.

A first positron fraction measurement from PAMELA was presented in 2009, with data collected up to February 2008 (see Ref. 5); recently, a new paper[6] has been published, containing data up to December 2008 (with an increase of 30% in statistics) and moreover a better understanding of systematic uncertainties related to the subtraction of p background: the new results are fully consistent with the previous ones, as shown in Fig. 3.

The positron fraction, as measured by PAMELA, is characterized by one order of magnitude improvement in statistics over previous measurements; besides, it covers the most extended energy range ever achieved by a single apparatus. The positron fraction above 10 GeV is in agreement with previous measurements but for the first time it clearly shows a significant increase with energy; this measurement had and is still having an unprecedented impact on the cosmic-ray community, since it can not be described in the framework of the standard theoretical predictions of sec-

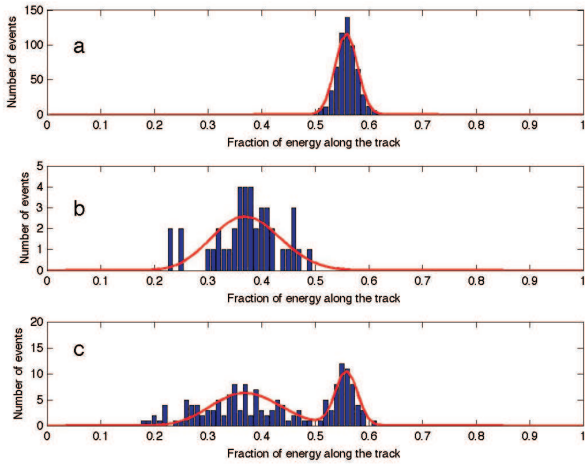

Fig. 2. Distribution of the fraction of energy measured in the calorimeter along the trajectory extrapolated from the spectrometer, for particles selected respectively as (a) electrons, (b) protons, (c) positrons, with the method outlined in the text, in the rigidity range 28–42 GV. In (c) the residual proton contamination (left) is clearly separated from the e^+ peak (right).

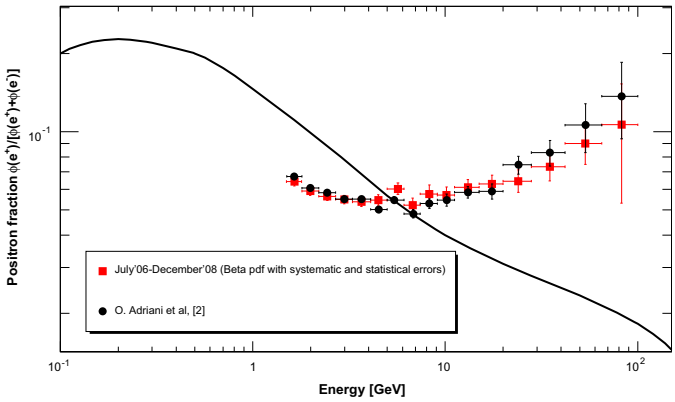

Fig. 3. Black points: the positron fraction measured by PAMELA as published in 2009.[5] Red points: the recently published new measurement,[6] where the vertical bars include both statistical and systematic errors, summed in quadrature. Line: a classical pre-PAMELA theoretical calculation[7] for pure secondary production of positrons during the propagation of cosmic rays in the galaxy. Figure from Ref. 6.

ondary production of positrons in the galaxy, even taking into account the large uncertainties in the models involved. Therefore either a significant modification in the theories of cosmic-rays acceleration and propagation is needed, or primary sources like dark-matter annihilation or astrophysical sources (e.g. pulsars), have to be taken into account.

At low energies the PAMELA positron fraction is lower than most of the other measurements, collected during the previous solar cycle; this is interpreted as the observation of a charge-dependent solar modulation effect, hypothesis supported by the fact that the PAMELA measurement is in agreement with the results of a contemporary balloon-borne experiment[8] which flew in June 2006 and also observed a similar positron fraction at low energies, but with much larger statistical uncertainties.

See e.g. Ref. 9 for a review of the possible interpretations of PAMELA positron data.

4. Antiproton analysis

The main issue to be faced in the antiproton analysis is the background of *spillover* protons, i.e. protons for which the charge sign is wrongly determined because of the uncertainty in the deflection measurement performed by the spectrometer. The *spillover* contamination is reduced to the desired level by introducing stronger selection criteria on the quality of the reconstructed trajectory (χ^2 and MDR), and by rejecting tracks with low-resolution position measurements related to noisy read-out channels or emission of δ-rays.

The first PAMELA measurement[10] of the $\overline{\mathrm{p}}/\mathrm{p}$ flux ratio, in the kinetic energy range 1.5–100 GeV, has been followed by a new publication[11] including more recent data and more refined analysis methods, extending the measurement down to 60 MeV and up to 180 GeV kinetic energies (see Fig. 4).

The higher energy limit of the new analysis is obtained by means of a looser (but still strong) MDR cut on the precision of the measured rigidity, i.e. requiring $\mathrm{R} < \mathrm{MDR}/6$ instead that $\mathrm{R} < \mathrm{MDR}/10$ (see Fig. 5); this is coupled to a refined study of the residual contamination from *spillover* protons: a fine-tuned simulation of the apparatus, including also variations with time of the detector performances, has been validated by comparing the distributions of several representative variables (e.g. coordinate residuals, χ^2 and covariance matrix for parameters of the track fit) with those obtained for *in-flight* data. The *spillover* background thus estimated is subtracted from the data and the discrepancy between the simulated and real

behaviour of the deflection distribution in the high-energy region is used to derive the residual systematic error.

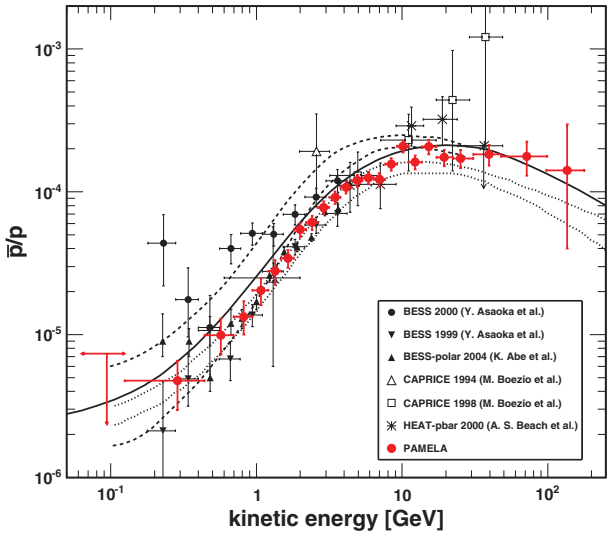

Fig. 4. Measurements of the antiproton/proton flux ratio from PAMELA and contemporary experiments; the lines represent different theoretical calculations for a pure secondary production of antiprotons during the propagation of cosmic rays in the galaxy. Figure from Ref. 11.

Other important issues are also taken into account in the antiproton analysis, e.g. the different calorimeter efficiency for p and $\overline{\mathrm{p}}$, the loss of particles in the instrument, the contamination from secondary pions produced in the materials above the spectrometer. For what concerns pions, a dedicated simulation has been validated by comparison with *in-flight* data below 1 GV, where pions are identified by relating the velocity and rigidity measurements from ToF and spectrometer, respectively; above 1 GV, the residual pion background is estimated to be negligible, apart from the range 1–3 GV where it is $\sim 10\%$ and hence is subtracted from the data.

The measured $\overline{\mathrm{p}}/\mathrm{p}$ ratio increases smoothly with kinetic energy up to about 10 GeV and then levels off. The data follow the trend expected from models of secondary production in the galaxy, but at the same time these results are enough precise to place strong constraints on theoretical calculations and on possible contributions from exotic sources, e.g. dark-matter particle annihilations. The new publication[11] also contains the first

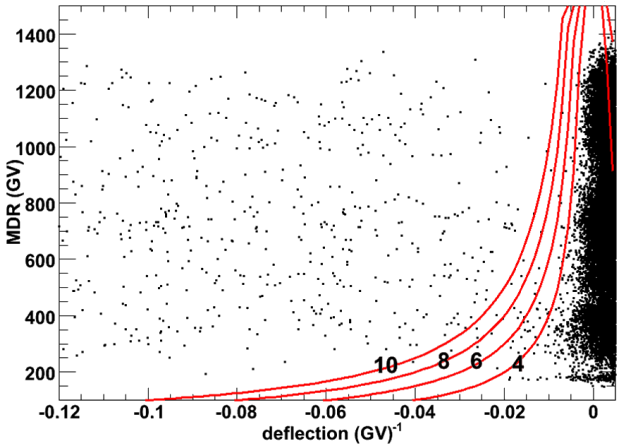

Fig. 5. Distribution in the η–MDR plane of a sample of selected antiproton and proton events before applying the event-dependent MDR cut. Events with negative η are mostly $\overline{\mathrm{p}}$; on the right side (positive η) the proton distribution is visible, with its *spillover* tail extending to negative deflections. The lines define different possible MDR cuts R<MDR/n (or equivalently MDR>n/$|\eta|$), with n = 10,8,6,4.

PAMELA measurement of the absolute antiproton flux. The additional issues concerning absolute flux measurements are illustrated in Sec. 5.

5. Absolute fluxes of Hydrogen and Helium

Cosmic-ray Hydrogen (mostly protons, with a $\sim 1\%$ deuterium component) and Helium ($\sim 10\%$ of H) are overwhelming with respect to other particle species; therefore pure samples of events can be obtained, which are not significantly affected by contamination backgrounds. In fact, this measurement of absolute flux is mostly affected by the instrumental systematics in the determination of the selection efficiencies and, above few hundreds GeV, in the spectrometer measurement of the particle rigidity; specifically, possible energy-dependent systematic biases, which can alter the shape of the measured spectra, have to be kept under control.

Given the performances of the PAMELA detectors, the purity of the *in-flight* collected samples of H/He and their high statistics (more than $\sim 10^8$ proton events), it has been possible to measure the absolute fluxes of H and He over more than three decades of rigidity, up to ≈ 1 TV, with an unprecedented total (statistical and systematic) precision of few %. This approach exploits the abundant *in-flight* acquired data to adequately characterize and minimize each single mechanism contributing to the instrumental sys-

tematics, with precision ranging from $\sim 0.1\%$ to few % over the energy range of interest.

A dedicated paper with the results of this work is currently in preparation; here only the main aspects of the analysis procedure are summarized and discussed. The PAMELA measurement of H and He fluxes will contribute to put further strong constraints on theoretical cosmic-ray models, and in particular to reduce the uncertainties on the calculations of the expected secondary antiparticles spectra. Moreover, most of the knowledge thus obtained on the PAMELA instrumental performances has been suitably exploited for the analysis of absolute fluxes of the other, much rarer, species ($\overline{\mathrm{p}}$, e^-, e^+, heavier nuclei).

5.1. *Selection efficiencies*

With the aim of obtaining a precise ($\sim$ %) measurement of the selection efficiencies, selection criteria have been grouped in subsets for which the efficiency can be directly measured with *in-flight* data; the small (not more than few %) instrumental biases introduced with this procedure are then corrected by means of the Monte Carlo simulation of the apparatus, validated through extensive cross-checks with *in-flight* collected data.

Concerning direct measurement of selection efficiencies with *in-flight* data, biases can arise from several mechanisms.

- **Inhomogeneities**. The dependence of a given selection-cut efficiency on time, particle energy and spatial/angular parameters of the trajectory in the geometrical acceptance of the apparatus, can affect the result, due to possible differences between time, energy or geometrical-acceptance composition of the data sample prepared for the efficiency measurement (indicated briefly as "efficiency data sample" in what follows) and the sample over which the selection cut is applied to obtain the flux.
- **Correlations**. Different selection cuts can be mutually correlated, i.e. each of them can have an efficiency, which is less than 100%, in the selection of the *same* specific category of H/He events. Therefore, to properly express the combined efficiency of all the above cuts as a product of single efficiency measurements, it is necessary that each affected category of events is included only in *one* of the corresponding "efficiency data samples".
- **Contaminations**. An "efficiency data sample", if not properly prepared, can contain spurious events, i.e. events which are by construction rejected by the selection cut whose efficiency is to be measured, and therefore

should not be part of the sample. Because of these contaminations, *in-flight* measured efficiencies can be underestimated.

Concerning Monte Carlo simulation of the apparatus, biases at the % level arise mostly from the practical limits to the possibility of building an accurate model including all the "fine" geometrical and physical characteristics of detectors and read-out electronics, and especially their possible variations with time, e.g. caused by changes of thresholds or gains or by failures of single sections.

The H/He selection cuts and the choice of fiducial geometrical acceptance have been fine-tuned to find an optimal compromise to minimize the net effect of all the different sources of instrumental systematics. Finally, several kinds of self-consistency checks have been performed on the whole procedure, with the specific purpose of estimating the residual systematic uncertainty in the efficiency measurement (shown in Fig. 6 together with other contributions):

- by varying the selections of "efficiency data samples" (the weights of the different inhomogeneity/correlation/contamination effects change, usually with conflicting trends);
- by using different time and energy bins;
- by cross-checking the stability of the high-rigidity flux (R $>$ 50 GV), for which solar modulation is negligible, obtained for different time intervals (months, years);
- by varying the fiducial acceptance; in particular, by cross-checking the measured flux with the one obtained with a restricted 10% acceptance corresponding to the inner part of the apparatus with respect to its cross-sectional plane.

5.2. *Rigidity measurement*

The uncertainty in the rigidity measurement performed by the spectrometer can cause a given event to be assigned to the wrong rigidity bin; because of the power-law behaviour of the spectra, this adds a spurious contribution to the flux measured for high-rigidity bins, which amounts to $\sim 1\%$ at 100 GV and $\sim 10\%$ at 1 TV, and is therefore not negligible for the H and He analysis.

This effect, varying from event to event with the MDR as discussed in Sec. 2, is accounted for in the measured spectra by means of a statistical unfolding approach based on the detailed simulation of the spectrometer:

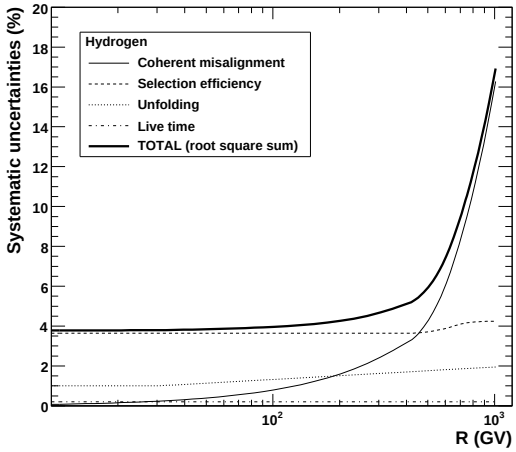

Fig. 6. The significant relative systematic uncertainties $\Delta\phi/\phi$ estimated in the PAMELA measurement of H flux ϕ, as a function of particle rigidity.

afterwards, the residual systematic error is estimated, which is mainly associated to the adopted unfolding technique.

Moreover, the uncertainty (~ 1 μm) of the spectrometer alignment procedure, implies that it can not account for a small "coherent" shift between the real and estimated positions of all the Si sensor planes; this spurious "bending" of the whole spectrometer system, in turn introduces a constant, event-independent shift $\Delta\eta$ in the measured deflections, or equivalently a $\Delta \mathrm{R} \approx \pm\Delta\eta \cdot \mathrm{R}^2$ in the measured rigidities for particles of negative/positive charge, respectively.

This "coherent misalignment" contribution is determined and corrected for by means of *in-flight* acquired samples of relativistic e^- and e^+, by comparing the distribution of energies resulting from the spectrometer and calorimeter measurement (taking into account possible emission of *brehmsstrahlung* photons in the spectrometer): while the calorimeter uncertainty does not depend on charge sign, the spectrometer energy measurement for e^- (e^+) is systematically lower (higher) because of the deflection shift superposed to the other random fluctuations ($\Delta\eta$ turns out to be negative). The limited e^+ statistics implies a residual uncertainty $\delta\eta \approx 1 \cdot 10^{-4}$ $(\mathrm{GV})^{-1}$ after the correction is applied; this is propagated on the measured flux and considered as an additional systematic uncertainty.

The "coherent misalignment" systematics estimated for the H flux is

shown in Fig. 6 together with the other main contributions. It is worth to note that the resulting overall systematic uncertainty in the H flux amounts to less than 5% up to 400 GV. Similar, even if slightly worse, results are obtained for He.

6. Conclusions and outlook

In this paper several aspects of the recent analysis work, done by the PAMELA collaboration, have been presented. The results of this work, i.e. the measurements of antiparticle (e^+ and $\overline{p}$) flux ratios and of H, He and $\overline{p}$ absolute fluxes, performed with unprecedented precision, constitute a further important step toward a better understanding of cosmic-ray physics.

Moreover, additional items, not discussed here, are currently under analysis and will be addressed in forthcoming publications. These include: the absolute fluxes of electrons, positrons and light nuclei; the study of solar modulation, affecting the low-energy end of the particle spectra, over a period of more than three years of data taking; the search for $\overline{He}$ events or other exotic signals (i.e. strangelets).

References

1. P. Picozza *et al.*, *Astropart. Phys.* **27**, 296 (2007).
2. R. Brun *et al.*, *Computer code GEANT*, version 3.21, CERN program library (1994).
3. A. Fassò *et al.*, *FLUKA: Status and Prospective for Hadronic Applications*, in *Proceedings of the MonteCarlo 2000 Conference*, Springer-Verlag, Berlin, 955 (2001).
4. M. Boezio *et al.*, *Astropart. Phys.* **26**, 111 (2006).
5. O. Adriani *et al.*, *Nature* **458**, 607 (2009).
6. O. Adriani *et al.*, *Astropart. Phys.* **34**, 1 (2010).
7. I.V. Moskalenko and A.W. Strong, *Astrophys. J.* **493**, 694 (1998).
8. J. Clem and P. Evenson, in *Proc. 30^{th} ICRC* (Merida, Mexico, 2007).
9. M. Boezio *et al.*, *New J. Phys.* **11**, 105023 (2009).
10. O. Adriani *et al.*, *Phys. Rev. Lett.* **102**, 051101 (2009).
11. O. Adriani *et al.*, *Phys. Rev. Lett.* **105**, 121101 (2010).